Self-Assembly of Organic Monolayers as Protective and Conductive Bridges for Nanometric Surface-Mount Applications

Ilia Platzman,[†] Hossam Haick,[†,‡] and Rina Tannenbaum*[,†,‡,§]

Department of Chemical Engineering and Russell Berrie Nanotechnology Institute, Technion—Israel Institute of Technology, Haifa 32000, Israel, and School of Materials Science and Engineering, Georgia Institute of Technology, Atlanta, Georgia 30332

ABSTRACT In this work, we present a novel surface-mount placement process that could potentially overcome the inadequacies of the currently used stencil-printing technology, when applied to devices in which either their lateral and/or their horizontal dimensions approach the nanometric scale. Our novel process is based on the "bottom-up" design of an adhesive layer, operative in the molecular/nanoscale level, through the use of self-assembled monolayers (SAMs) that could form protective and conductive bridges between pads and components. On the basis of previous results, 1,4-phenylene diisocyanide (PDI) and terephthalic acid (TPA) were chosen to serve as the best candidates for the achievement of this goal. The quality and stability of these SAMs on annealed Cu surfaces (R_{rms} = 0.15−1.1 nm) were examined in detail. Measurements showed that the SAMs of TPA and PDI molecules formed on top of Cu substrates created thermally stable organic monolayers with high surface coverage (~90%), in which the molecules were closely packed and well-ordered. Moreover, the molecules assumed a standing-up phase conformation, in which the molecules bonded to the Cu substrate through one terminal functional group, with the other terminal group residing away from the substrate. To examine the ability of these monolayers to serve as "molecular wires," i.e., the capability to provide electrical conductivity, we developed a novel fabrication method of a parallel plate junction (PPJ) in order to create symmetric Cu-SAM-Cu electrical junctions. The current-bias measurements of these junctions indicated high tunneling efficiency. These achievements imply that the SAMs used in this study can serve as conductive molecular bridges that can potentially bind circuital pads/components.

KEYWORDS: copper • self-assembled monolayer • surface-mount technology • terephthalic acid (TPA) • 1,4-phenylene diisocyanide (PDI) • molecular electronics

1. INTRODUCTION

Surface mount technology (SMT) involves the use of the stencil-printing process for ultra-large-scale integration (ULSI) technology in which a thin layer of solder paste, made by a fine mixture of solder powder with viscous acid flux, is deposited on copper (Cu) pads, followed by positioning of the components onto their designated places (1, 2). Although this technology can be applied successfully in the macro- and microscale regimes (3), it fails when either the lateral and/or horizontal device dimensions approach the nanometric scale. This failure occurs because the component placement accuracy is affected by the height, area, or volume of the solder-paste bricks (3); by the lateral mobility of the components during the placement and reflow processes (4, 5); by the cracking of solder-paste attachment during cyclic thermal loadings (6); and by the corrosive nature of the flux residues (7). In addition to these difficulties, there are two main problems associated with the use of Cu in this context: (i) formation of relatively rough Cu surfaces (~5 nm roughness), which would make the effective contact much smaller than their geometrical cross-sectional area (8); and (ii) formation of Cu-oxide layers upon exposure to air (8−13), which would induce trap states at the Cu/Cu-oxide interface leading to a significant degradation in its interconnection capability, which, in turn, could cause electrical malfunctions (14, 15). It is therefore expected that the current SMT will soon reach its maximum capability to accommodate the growing needs of the industry and the shrinking size of the components, and as a consequence, component density would reach saturation as well. Therefore, there seems to be an urgent need for a novel design that will override the current technology. Hence, the overall goal of our work is to develop a new concept for a surface-mount placement process that will be based on a "bottom up" design of a conductive and protective adhesive layer through the use of molecules with "tailored" properties and functionalities that would bind to metallic surfaces, i.e., nanopads, on one side and to nanocomponents on the other side, forming a protective, bridging and conductive layer, operative in the nanometric regime, as schematically described in Figure 1.

The development of such a concept depends on three main factors: (i) the control of the morphology and oxidation of the Cu surfaces, (ii) the optimization of the self-assembled monolayer (SAM)/Cu system both in terms of the type of

* Corresponding author. E-mail: rinatan@technion.ac.il and rinatan@mse.gatech.edu.

Received for review May 15, 2010 and accepted August 12, 2010

[†] Department of Chemical Engineering, Technion—Israel Institute of Technology.

[‡] Russell Berrie Nanotechnology Institute, Technion—Israel Institute of Technology.

[§] Georgia Institute of Technology.

DOI: 10.1021/am100427a

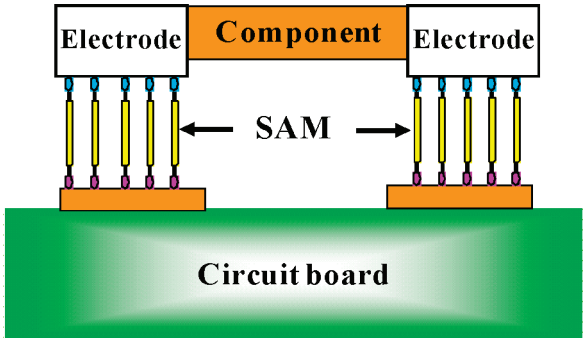

FIGURE 1. Idealization of SAM as conductive and mechanical bridges for nanometric surface-mount applications.

molecules used and in terms of the extent of coverage and protection against Cu substrate oxidation, and (iii) the creation of stable and highly ordered SAM, binding of the SAM to a metallic overlayer and investigation of the efficiency of molecular conductivity.

Recent developments in our laboratories have shown the ability to satisfy the requirements of the first two factors toward developing of a new concept for the surface-mount placement process. More specifically, we have shown the ability to prepare and to control high-quality, defect-free, ultrasmooth polycrystalline Cu surfaces (R_{rms} = 0.15−1.1 nm) by employing an annealing modification and, in turn, to achieve superior oxidation resistance of the Cu surfaces (8, 13). The results showed a significant increase in the grain size of the Cu surface structure from 20 × 60 nm to 300 × 300 nm and decrease in the separation between grain boundaries for annealed Cu surfaces, this in agreement with the previously published theoretical investigations which pointed out the energetic advantages of annealed metal surfaces (16−22). The oxide layer thickness of annealed Cu surfaces was ∼30% lower in comparison to nonannealed polycrystalline Cu samples at similar exposure conditions (13). In parallel, we have shown that symmetric difunctional molecules on Cu substrates could serve as excellent candidates for protective organic coatings for ULSI technology (23, 24). The results of this study indicated that isocyanides, thiol, and carboxylic functional groups provide the strongest adhesion to ambient copper surfaces. Moreover, it was shown that molecules such as 1,4-phenylene diisocyanide (PDI) and terephthalic (TPA) acid adopted "standing-up" phase configuration, in which they bonded to the Cu substrate through only one terminal functional group, with the other terminal group disposed away from the Cu substrate. Consequently, the ability of the TPA and PDI SAMs to prevent the oxidation of the underlying annealed Cu during storage in ambient air conditions were examined, both qualitatively and quantitatively for long time periods (<110 days) (8, 25). The TPA-modified Cu surfaces have not shown any detectible oxidation during the first two weeks of exposure. The protection efficiency of both TPA and PDI layers were found to be considerably superior to those reported earlier with n-alkanethiols SAM on polycrystalline Cu surfaces (26−29).

In this study, we will address two main avenues of action to complete the nanoscale-based SMT concept. The first is the preparation of high-quality, defect-free, and homogeneous SAMs of PDI and TPA molecules on annealed Cu surfaces. The second is construction of top metallic Cu layer (mimicking the "component") by employing a "sandwich" approach, in order to assess the ability of these SAMs to serve as "molecular wires," i.e., the capability to provide electrical conductivity (30−36). All samples, were characterized by the novel parallel plate junction (PPJ) method which was developed in order to create symmetric Cu-SAM-Cu electrical junctions. This method allowed the characterization of the SAMs conductive properties in a simple and reproducible manner by minimization of the possible junction defects as shorts and SAM's damage.

2. EXPERIMENTAL SECTION

2.1. Materials. Tantalum (Ta) and copper (Cu) metals with >99% purity were purchased from Kurt J. Lesker, USA. N-type, phosphorus-doped (0.008−0.020 Ω cm resistivity), two-inch, single-side-polished Si (100) wafers with <1 nm roughness were purchased from Virginia Semiconductor Inc., USA. $NH_4F_{(aq)}$ 40% and $HF_{(aq)}$ 40% were purchased from Sigma-Aldrich and Merck, respectively. Water rinses used 18 MΩ deionized (DI) water obtained from a Millipore Nanopure system. Methanol, acetone, dichloromethane and 1,1,1-trichloroethane were purchased from Frutarom Ltd., Israel. 1,4-Terephthalic acid (TPA) $CO_2H-C_6H_4-CO_2H$ and 1,4-phenylene diisocyanide (PDI) CN-C_6H_4−NC with 98 and 99% chemical purity, respectively, were purchased from Sigma Aldrich. Tetrahydrofuran (THF) and toluene supra dry solvents were purchased from Bio Lab Ltd., Israel.

2.2. Sample Preparation. Prior to metal evaporation, all Si (100) wafers were cleaned by sequential rinsing with DI water, methanol, acetone, dichloromethane, 1,1,1-trichloroethane, dichloromethane, acetone, methanol, and DI water. Samples were then dried under a stream of $N_{2(g)}$ and treated with ozone oxidation for 20 min in a UVOCs apparatus. The native oxide was etched by immersing the clean wafers in buffered $HF_{(aq)}$ (pH = 5−6, 5:1 (v/v) $NH_4F/HF_{(aq)}$) for 30 s, while agitating the solution for preventing formation of etch pits. At the end of the etching process, the samples were rinsed thoroughly with 18 MΩ DI water for 30 s, dried under a stream of nitrogen, and transferred directly to a reactive sputtering system (LS-320S, Von Ardenne, Germany) for deposition of 20 ± 5 nm tantalum nitride (TaN) films. The TaN layer serves as an effective barrier for reducing Cu diffusion into the SiO_2/Si substrate during the annealing at elevated temperature (<700 °C) (37, 38). The deposition of TaN films was carried out at 1 × 10^{-7} Torr base vacuum and applying a power of 50 W and a sputtering pressure of 15 mtorr (6 sccm N_2 and 12 sccm Argon). The TaN-coated Si samples were then transferred to a dry nitrogen glovebox (<0.6 ppm O_2 and <0.1 ppm H_2O) (MBRAUN, Labmaster 130, USA) connected with an e-beam evaporator (TFDS-870, Vacuum Systems & Technologies Ltd., Israel), heated to 300 °C at 1−5 × 10^{-6} Torr and coated with 300 ± 10 nm Cu films, using <1 Å/s deposition rate. Immediately after Cu deposition, the substrates were annealed at 580 °C and 2 × 10^{-7} Torr for a period of 8 h, to minimize the Cu surface roughness (8, 37, 38). Following the annealing procedure the samples were carefully removed from the tray holder of the e-beam evaporator, and broken into a number of pieces for further self-assembly procedures.

All adsorption solutions were prepared in new glassware that was first cleaned by rinsing and sonicated in DI water, acetone, and pure THF or toluene solvents. The TPA and PDI at concentrations of 1.0 mM were dissolved in the THF and toluene solvents, respectively, and sonicated in order to prevent the possible molecular agglomeration. The SAMs of TPA and PDI were formed inside the dry nitrogen glovebox by immersing

the freshly prepared, annealed Cu samples in the solutions for immersion times of 24 and 8 h for TPA and PDI, respectively. Then the samples were removed from the adsorption solution, rinsed and sonicated for 1 min in pure solvents in order to remove all loosely bound molecules and dried under a stream of N_2(g). Thereafter, the TPA- and PDI-modified Cu samples were exposed to ambient air conditions during and between the various characterization steps.

2.3. Polarization Modulation Infrared Reflection Absorption Spectroscopy (PM-IRRAS). PM-IRRAS spectra were collected on Nicolet 8700 Nexus (Thermo Electron Corporation, USA) with a PM-IRRAS attachment including a PEM-90 photoelectric modulator (Hinds) and a N_2 cooled MCT detector at near grazing angle of 88° relative to the surface normal. The measurements were collected under the dry air purging conditions. An average of 2000 scans per analysis was collected, with the resolution of 2 cm^{-1}. Reflectance spectra are expressed $\Delta I/I = 100 \times (I_s - I_p)/(I_s + I_p)$, converted to arbitrary units. I_p and I_s designate the spectra collected parallel and perpendicular to the plane of incidence, respectively (39).

2.4. Spectroscopic Ellipsometery (SE). To measure the thickness of the organic layers, were recorded ellipsometric spectra over a range from 250−1000 nm at three different incidence angles 65, 70, and 75° using a spectroscopic phase modulated ellipsometer (M-2000 V Automated Angle, J. A. Woollam Co., Inc., USA). For TPA- and PDI-modified Cu samples we used a three-phase SAM/(Cu_2O+CuO)/Cu substrate model to extract the thickness of the SAM layer. An adsorption-free Cauchy dispersion of the refractive index with values ranged from 1.46 to 1.61 at 1000 and 250 nm, respectively, was assumed for SAM layer (40). The optical constants of the Cu and Cu_2O were determined experimentally from the reference samples. All layer thicknesses reported were calculated after averaging at least five measurements.

2.5. X-ray Photoelectron Spectroscopy (XPS). Surface analysis of the molecularly modified Cu samples was performed by XPS, using a Thermo VG Scientific, Sigma Probe, (UK), operating at a base pressure of $<3 \times 10^{-9}$ Torr and fitted with a monochromatized Al Kα (1486.6 eV) X-ray source. No reduction of the surface was observed during prolonged exposure of oxide surfaces to the monochromatized beam of 100W X-ray beam of 400 μm in diameter (41). Broad scan survey spectra and high-energy resolution spectra of Cu LMM, Cu2p, C1s, N1s, and O1s were collected at pass energies of 100 and 20 eV, respectively. The measurements were performed in the bulk sensitive mode at a take-off angle, $\theta = 65°$, between the direction of an analyzer and the specimen plane. Spectral analysis was performed using the peak fitting software (XPS-PEAK version 4.1) after a Shirley background subtraction (42). Peak fitting solutions were sought for $\chi^2 < 2$, where χ^2 is the standard deviation.

2.6. Ultra High Vacuum Scanning Tunnelling Microscope (UHV-STM). STM measurements were performed using a UHV/VT STM Omicron system (Germany) equipped with a tungsten tip, which was cleaned in UHV by electron bombardment to remove the tungsten oxide prior to use. All STM images were obtained at selected conditions (constant bias voltage of 2 V and a tunneling current of 20−60 pA), such that no STM tip induced surface diffusion could take place during the scans between the tip and the sample (43).

2.7. Current Density vs Bias ($J-V$) Measurements. To reliably measure the conductive properties of Cu-SAM-Cu junctions, we developed a novel fabrication parallel plate junction (PPJ) method. This method guarantees good control over the device area and intrinsic contact stability, and produces a large number of devices with acceptable yield. Two features were essential to the measurement system, the first of which was the employment of annealed ultra smooth and highly stable Cu bottom and top contact surfaces, and the second feature was

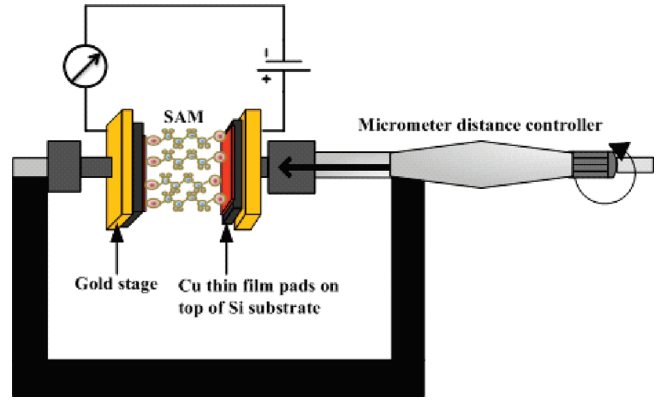

FIGURE 2. Schematic view (not to scale) of the parallel plate junction (PPJ) method of fabrication.

the fine controlled contact between the parallel Cu-SAM and Cu bare surfaces in order to minimize such defects as impurities, oxidation and grain boundaries that have a high potential to influence on the ($J-V$) characteristics and in order to minimize the damage to SAM during the physical contact between the bare and molecularly modified Cu surfaces, respectively. A schematic representation of the device structure is illustrated in Figure 2 and the fabrication details are presented in the following paragraph.

Freshly prepared molecularly modified and bare Cu samples (see experimental section 2.2.) were contacted on the back of a Si substrate to the conductive gold stages by applying the thin layer of silver-filled epoxy (EPO-TEK-EE-129-4, 0.0003 Ω cm resistivity, Electron Microscopy Sciences, USA) after curing at 70° for 2 h in a dry nitrogen glovebox (<0.1 ppm O_2 and <0.1 ppm H_2O). To create the thin, smooth, and homogeneous layer (100 ± 10 nm), the mixture of silver-filled conductive epoxy was spin-coated on the gold stages for 30 s at a spin rate of 1000 rpm. For all samples, the exposure to ambient was limited to ca. 5 min prior to the transfer into the glovebox. The fine contact between the molecularly modified and bare Cu surfaces was achieved using the micrometer distance controller and online $J-V$ measurements of a Agilent B1500A semiconductor device analyzer (Agilent Technologies, UK) under optical microscope observation. To prevent any pressure on the Cu surfaces during the contact, the PPJ method was developed in such a manner that one of the sample stages (the right one in Figure 2) was free to move 2 mm in X direction, while the second stage was static. The connection between the device analyzer and the measured PPJ system was provided by triax cables in order to prevent the possible current leakage. Most scans were carried out between −1 V and +1 V in a swap mode and were done several times for each junction with a scan rate of 10 mV s^{-1}. To neglect the influence of water and other adventitious contaminants from the ambient air, all current-bias ($J-V$) measurements were carried out in ultradry glovebox conditions.

3. RESULTS AND DISCUSSION

3.1. Surface Analysis. For the qualitative investigation of the TPA-modified Cu surfaces we used the information obtained from high resolution XPS spectra of C1s, O1s, $Cu2p_{3/2}$ and Cu LMM as shown in Figure 3A−D, and summarized in Table 1. In the peak fit for C1s, shown in Figure 3A, there are four peaks at 284.3 eV (peak 1), 285.2 eV (peak 2), 286.6 eV (peak 3), and at 288.9 eV (peak 4), corresponding to aromatic carbons, carbons adjacent to carboxylic acid group, carbons in carboxylate groups bonded to the Cu and carbons in free carboxylic acid groups, respectively (44−46). The peaks area ratio (see Table 1) matched the stochiometric

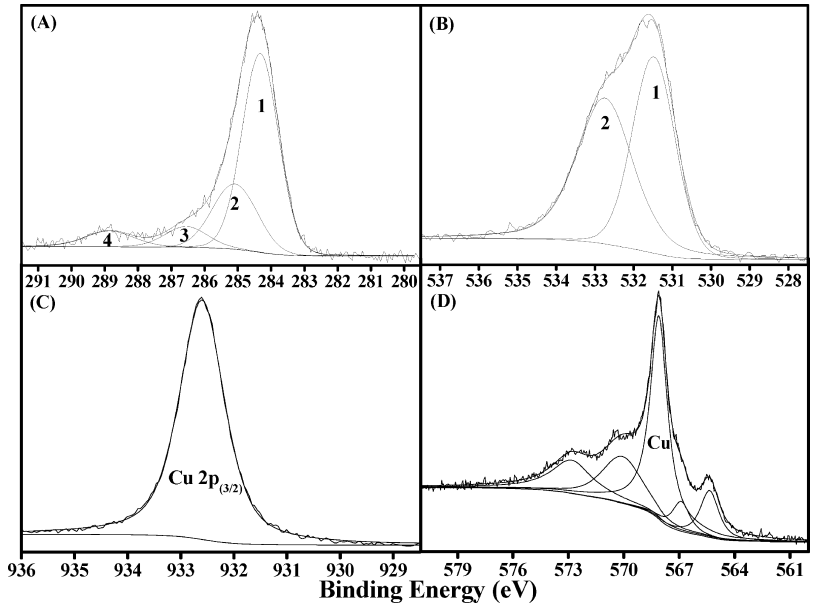

FIGURE 3. (A) C1s, (B) O1s, (C) Cu 2p3/2, and (D) Cu LMM spectra for TPA molecularly modified, polycrystalline, and annealed copper surface measured 1 h after exposure to ambient air. For the sake of clarity of presentation the peak fitting data summary for the spectra presented in this figure is presented in Table 1.

Table 1. Summary of Peak Fitting Parameters for TPA Molecularly Modified, Polycrystalline, Annealed Copper Surface Spectra As Presented in Figure 3

spectrum	peak	binding energy (eV)	fwhm (eV)	intensity (a.u.)
C1s	1	284.3	1.29	1506
	2	285.2	1.58	740
	3	286.6	1.50	310
	4	288.9	1.70	270
O1s	1	531.5	1.35	1083
	2	532.7	1.70	1215
$Cu2p_{3/2}$	Cu	932.7	1.01	9492
Cu LMM	Cu	568.0	1.13	2365

ratio of the different carbons in TPA molecules, which indicated that the organic film layer was deposited with a high degree of specificity and very limited adventitious contamination from air. In the O1s spectrum, shown in Figure 3B, there are two peaks at 531.5 eV (peak 1) and 532.7 eV (peak 2), corresponding to a carboxylate group bonded to the Cu and a free carboxylic group, respectively (47). O1s chemical shifts are usually not large, therefore it is possible that due to the relatively high value of its fwhm value, two unresolved oxygen species are present within the peak at 532.7 eV (see Table 1) (48). It may be prudent at this point to mention that there was no evidence of an oxygen peak at 530.4 eV, which would be attributed to a native Cu_2O layer. High-resolution $Cu2p_{3/2}$ and Cu LMM spectra shown in Figure 3C and 3D, respectively, were collected in order to investigate the oxidation state of the molecularly modified Cu surfaces. In agreement with the O1s spectra and our previous wor k (8), no Cu_2O and CuO layers were observed. The $Cu2p_{3/2}$ spectrum (see Figure 3C) showed only one peak at 932.7 eV with fwhm of 1.01 eV, corresponding most likely only to Cu metal, in a good agreement with the spectrum of sputtered oxide-free and oxygen-free $Cu2p_{3/2}$ (8, 13). In the peak fit of Cu LMM, shown in Figure 3D, there is one major peak at 568.3 eV (Cu metal) and four other peaks at 570.5, 573.0, 567.1, and 565.2 eV that represent different transitions states of the Cu LMM spectrum (49).

The high-resolution XPS spectra of C1s, N1s, $Cu2p_{3/2}$, and Cu LMM were used to examine the quality of the PDI-modified Cu surfaces as shown in Figure 4A–D, respectively, and summarized in Table 2. In the peak fit for C1s, shown in Figure 4A, there are three binding energy peaks at 284.8 eV (peak 1), 285.7 eV (peak 2) and a relatively broad binding energy peak at 286.7 eV (peak 3), corresponding to aromatic carbons, to carbon atoms adjacent to isocyanide groups and to carbon atoms of both bonded and free isocyanide groups, respectively (44, 45). Figure 4B shows the peak fitting for the N1s spectrum, where two peaks with similar intensities (see Table 2) were observed at 399.6 eV (peak 1) and at 401.6 eV (peak 2), corresponding to nitrogen atoms belonging to bonded and free isocyanide groups, respectively. The relatively strong upward binding energy shift of the free isocyanide group relatively to the bonded group (~2 eV) can be attributed mainly to the fact that the nitrogen in a free isocyanide group has a partial positive charge compared to the negative charge on the carbon atom, because its lone pair electrons are involved in the bond with the carbon, causing the nitrogen to be essentially quarternized (i.e., having 4 bonds) (44, 50). The $Cu2p_{3/2}$ spectrum, shown in Figure 4C, exhibits two resolved peaks at 932.6 eV and at 933.3 eV, corresponding to Cu metal and to Cu-Isocyanide bond, respectively (44). The presence of a native Cu oxide layer (e.g., Cu_2O) at 932.6 eV can be neglected due to the small value of the fwhm (1.03 eV), which indicates that this peak should be attributed to Cu metal only. Peak fitting of the Cu LMM spectrum, shown in Figure 4D, exhibits one major difference in comparison to Cu LMM spectrum of TPA-modified Cu surfaces, namely, a peak at 572.1 eV, which is

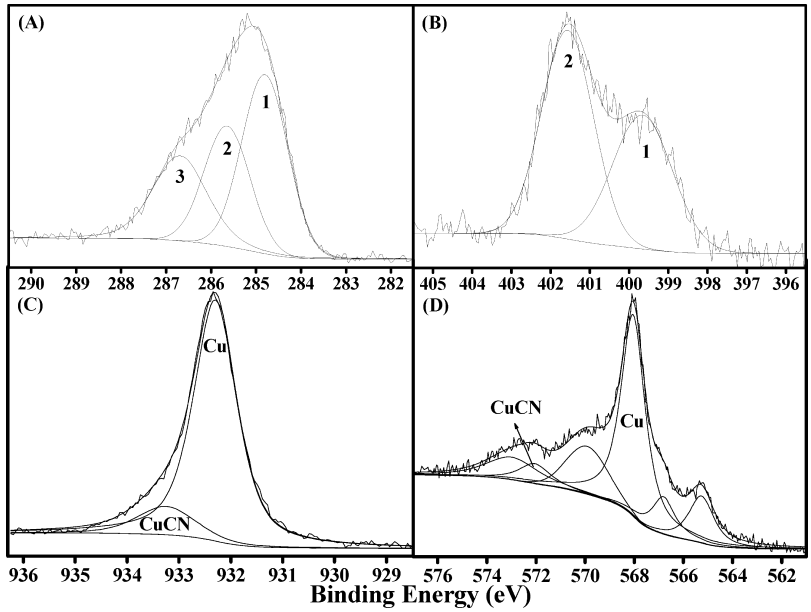

FIGURE 4. (A) C1s, (B) N1s, (C) Cu 2p3/2, and (D) Cu LMM spectra for PDI molecularly modified, polycrystalline, and annealed copper surface measured 1 h after exposure to ambient air. For the sake of clarity of presentation, the peak fitting data summary for the spectra presented in this figure is presented in Table 2.

Table 2. Summary of Peak Fitting Parameters for PDI Molecularly Modified, Polycrystalline, Annealed Copper Surface Spectra As Presented in Figure 4

spectrum	peak	binding energy (eV)	fwhm (eV)	intensity (a.u.)
C1s	1	284.8	1.20	1526
	2	285.7	1.22	879
	3	286.8	1.45	818
N1s	1	399.6	1.80	470
	2	401.6	1.55	520
$Cu2p_{3/2}$	Cu	932.7	1.03	9220
	CuCN	933.3	1.30	1324
Cu LMM	Cu	567.9	1.12	2151
	CuCN	572.1	1.50	203

attributed to a Cu-Isocyanide bond (44). Similarly to the TPA-modified Cu surface, the Cu LMM spectrum of the PDI-modified Cu surface shows no evidence of oxidation.

UHV-STM images were used to confirm the morphology of the TPA and PDI organic layers on top of the Cu surface. Images A and B in Figure 5 show representative UHV-STM 2D images of the phase formed in the self-assembly process of TPA and PDI molecules on annealed Cu thin film surfaces, respectively. Both images show similar morphology in which most of the surface (>85%) is covered with large islands consisting of a self-assembled layer of densely packed molecules, separated by interisland regions (such as pinholes, which consist of molecule-free domains, dark islands) having 5−10 nm in diameter. The relatively low surface root-mean-square roughness (R_{rms}) values of 0.62 and 0.55 nm in TPA and PDI images, respectively, are mainly attributed to the homogeneous morphology of the organic layers adsorbed on energetically stable, ultrasmooth, annealed Cu surfaces, without any evidence of agglomeration of these molecules and with minimum number of pinhole regions. The UHV-STM cross-section profile of the molecular "domains" of 0.9 ± 0.1 nm for TPA and 0.7 ± 0.1 nm for PDI showed comparable thickness values to those obtained by SE measurements of 1.10 ± 0.05 nm and 0.86 ± 0.03 nm on the same TPA- and PDI-modified Cu surfaces, respectively. These thicknesses are closely consistent with the theoretical thicknesses of TPA and PDI monolayers in which the molecules adopt a standing-up conformation during the self-assembly process such that only one terminal functional group bonds to the Cu substrate through, whereas the other group is directed away from the substrate surface.

To assess the stability of the SAMs at elevated temperatures, the surfaces were heated to 200 °C for 1 h inside the UHV-STM system. Images C and D in Figure 5 show representative UHV-STM 2D images of the phase formed through the self-assembly process of TPA and PDI molecules on annealed Cu thin film surfaces after heating to 200 °C, respectively. In comparison to the nonheated surfaces, the morphologies of heated surfaces exhibited slightly higher R_{rms} values, 0.73 and 0.66 nm for TPA- and PDI-modified Cu, respectively. These higher values can be attributed mainly to slightly larger pinhole areas because of the non-significant molecular desorption during the heating modifications. However, more than ∼80% of the surface is still covered by the SAMs in both cases, a fact that is most likely responsible for the strong coordinative reaction between the PDI and TPA functional groups and Cu surface atoms, as can be observed also from PM-IRRAS measurements, see the following paragraph.

To confirm the standing-up conformation of the TPA and PDI SAMs, we used information obtained from PM-IRRAS measurements. The representative PM-IRRAS spectra of the organic monolayers generated by the self-assembly of a 1 mM PDI solution for 8 h and a 1 mM TPA solution for 24 h on annealed copper substrates are presented in panels A and B in Figure 6, respectively. In Figure 6A, there are four major peaks at 1506, 1604, and 2121 cm^{-1} and 2158 cm^{-1},

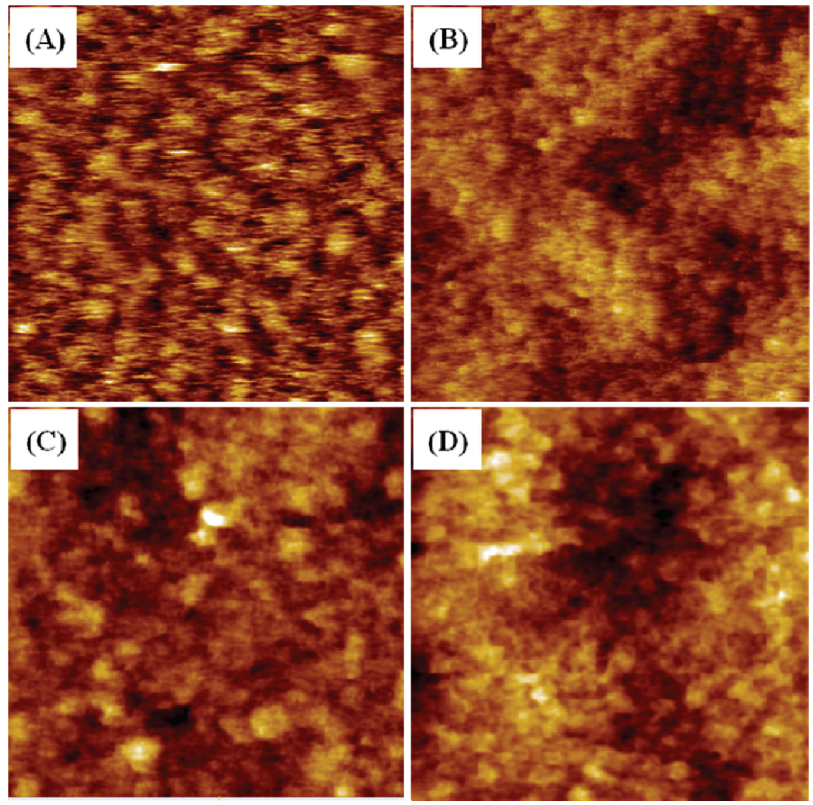

FIGURE 5. UHV-STM 2D representative images showing the phase formed in the self-assembly process of (A) TPA and (B) PDI on annealed Cu surfaces. (C, D) Images showing the same TPA- and PDI-modified annealed Cu surfaces, respectively, after heating to 200 °C. The scales in all images are 125 nm × 125 nm and R_{rms} values of 0.62, 0.53, 0.73, and 0.66 nm were measured for A−D, respectively.

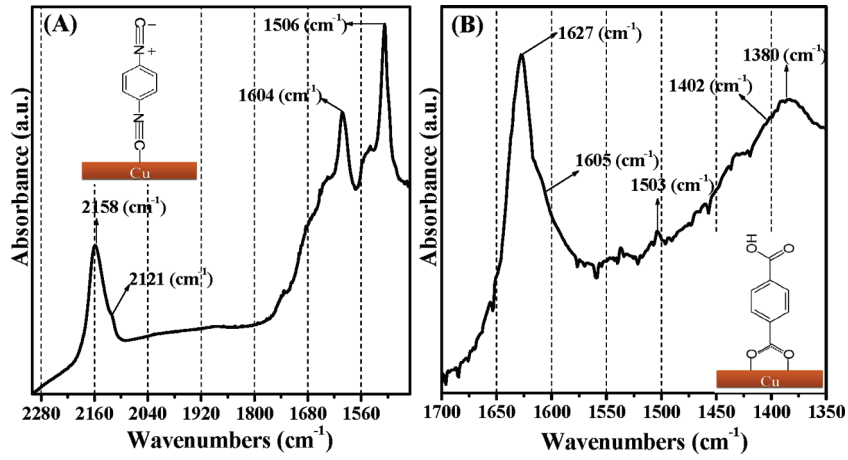

FIGURE 6. PM-IRRAS spectra of (A) 8 h self-assembled PDI 1 mM, and (B) 24 h self-assembled TPA 1 mM on annealed copper substrate (see Experimental Section) after 1 h of exposure to ambient air. The insets show the schematics of the chemical structures of PDI and TPA molecules on top of the Cu surface.

attributed to the vibration along the long axis of the phenyl ring, to the in-plane vibration mode of the phenyl ring and to the symmetric stretch of free isocyanide group and isocyanide group bonded to the Cu substrate, respectively (23, 51−54). It is important to mention here that there were no detectable peaks in the 1680−1700 cm^{-1} spectral range, which would have been indicative of the presence of an imine stretch (52), and hence, it is unlikely that the isocyanide groups could have undergone rehybridization (i.e., conversion of the NC triple bond to a double bond) or oligomerization (55−57). The absence of the imine peak in the PM-IRRAS spectrum is consistent with the high resolution N1s XPS spectrum (see Figure 4B), in which no evidence of an imine nitrogen at 398.6 eV was observed either. The fact that the bonded isocyanide group is strongly blue-shifted (by ∼48 cm^{-1}), whereas the free group has a less pronounced shift, as compared to the position of the non-adsorbed isocyanide group (2110 cm^{-1}) suggests that the isocyanide groups are no longer equivalent in the adsorbed state, and therefore, PDI is adsorbed on Cu mainly through one isocyanide group with the other isocyanide group disposed away from the surface. The strong blue-shift can be attributed to the antibonding character of the carbon lone pair electrons in the isocyanide bond, and to the increased

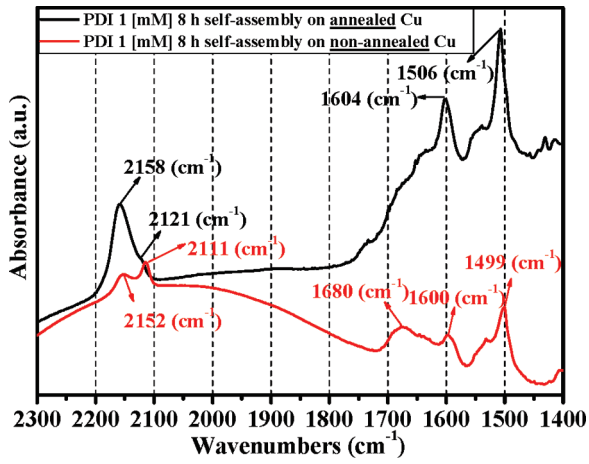

FIGURE 7. PM-IRRAS spectra of the PDI 1 [mM] after 8 h of self-assembly on annealed (above spectrum) and nonannealed Cu surfaces (bottom spectrum). NOTE, that the SAMs were prepared and measured in the same conditions (i.e., self-assembly time, concentration, and similar environment), the only difference being the Cu annealing.

stretch of this bond upon "donation" of these electrons to Cu (50, 51). Figure 5B shows a representative PM-IRRAS spectrum of TPA-modified Cu surfaces, consisting of peaks at 1380, 1402, 1503, 1605, and 1627 cm^{-1}, corresponding to the symmetric stretch of free carboxylate ions, the symmetric stretch of bonded carboxylate ions to the Cu surface, the vibration along the long axis of the phenyl ring, the antisymmetric stretch of free carboxylate ions with the contribution of the in-plane vibration mode of the phenyl ring at 1600 cm^{-1} and the antisymmetric stretch of bonded carboxylate ions to the Cu substrate, respectively (23, 52, 58). Similar to PDI, the observed blue-shift of the symmetric and antisymmetric stretch peaks of bonded carboxylate ions can be attributed to the increased strength of the carboxylate group bonds due to the coordination reaction with the Cu upon the adsorption. The different chemical environment of the bonded carboxylate ions compared to the free carboxylate ions of the coordinated TPA molecules is consistent with the high resolution C1s XPS spectrum shown in Figure 3A (peaks 3 and 4).

Figure 7 shows the PM-IRRAS spectra of the PDI on annealed (top spectrum) and nonannealed Cu surfaces (bottom spectrum) in order to emphasize the essential impact of the annealing process of the Cu surfaces on the formation of homogeneous SAMs. Note that the PDI-modified Cu surfaces were prepared and measured at the same conditions described previously (i.e., assembly time, solution concentration, and environmental conditions), with the only difference being the annealing process of the Cu surfaces. As can be seen, the spectra are different in terms of the relative intensities and peak locations. This difference can be explained by the possible agglomeration and partial polymerization of the PDI layer on nonannealed Cu. This agglomeration is supported by the fact that the intensity of the free isocyanide group absorption peak is higher compared to intensity of the bonded isocyanide peak. Moreover, the free isocyanide peak is red-shifted to 2111 cm^{-1}, which is almost identical to the stretching vibration of the free-state, unabsorbed isocyanide molecule (52, 59, 60). The average thickness of the SAM obtained by SE measurements was of 4 ± 0.05 nm, which is consistent with the agglomeration mechanism. Partial polymerization of the PDI was also observed on nonannealed Cu surfaces, as evidenced by the appearance of a new peak at 1680 cm^{-1}, corresponding to imine groups, formed as a result of rehybridization (55). The different conformations of the organic layers inferred from the PM-IRRAS spectra can be solely attributed to the different morphologic (e.g., roughness, grain dimensions, crevices) and energetic properties (e.g., grain boundary energies) of the annealed and nonannealed Cu surfaces.

Taken together, these observations are consistent with the formation of dense, homogeneous, and stable TPA and PDI SAMs that adopt a standing-up phase conformation. Such advantages as small pinhole areas together with low-defect, oxide-free and ultrasmooth properties of the molecularly modified annealed Cu surfaces, led these SAM-Cu systems to serve as a good candidates as organic, nanoscale, conductive and protective bridges for surface mount placement processes. The conductive properties of these monolayers have been studied and discussed in the following paragraphs.

3.2. Cu-SAM-Cu Junctions. The critical step in the fabrication of large-area molecular junctions is applying the metal top electrode. The direct, vacuum metal evaporation creates shorts and damages the SAM due to the filamentary growth of noble metals (61−65), SAM exposure to elevated temperatures and high kinetic energies of the impinging atoms/clusters (66−68). The indirect vacuum evaporation of metals (65, 69), electrochemical metal deposition (70−76) and printing-type approaches (77−79) have some clear technological possibilities. However, such disadvantages as very low deposition efficiency (69), penetration through the SAM defect sites due to the presence of large amounts of free metal ions in addition to the three-dimensional metal clusters growth (72−76), and generally poor electronic quality (e.g., ~20% yield) (80) hinder the reproducible work with these methods. In this context, construction of top metallic Cu layer with these methods becomes nonefficient and very complicated. To overcome these difficulties, we developed a new PPJ method to create symmetric Cu−SAM−Cu electrical junctions.

Figure 8 illustrates the typical $J-V$ characteristics of Cu−Cu and Cu−SAM−Cu junctions, 0.19 cm^2 in area, contacted by the PPJ method. As can be observed, the current in Cu−Cu junction exhibits typical Ohms law characteristics and its current is orders of magnitude larger in comparison to the Cu−SAM−Cu junctions. The current in the molecularly modified junctions is dominated by the PDI and TPA monolayers without any contribution from the Cu oxide layer. This layer was shown to be absent, as evidenced by the XPS results (see the XPS results discussions in the previous section). Both SAM-modified junctions show, as expected, almost similar $J-V$ characteristics, due to the similar properties of both adsorbed PDI and TPA molecules in terms of length (i.e., the tunnelling barrier), π-conjugated

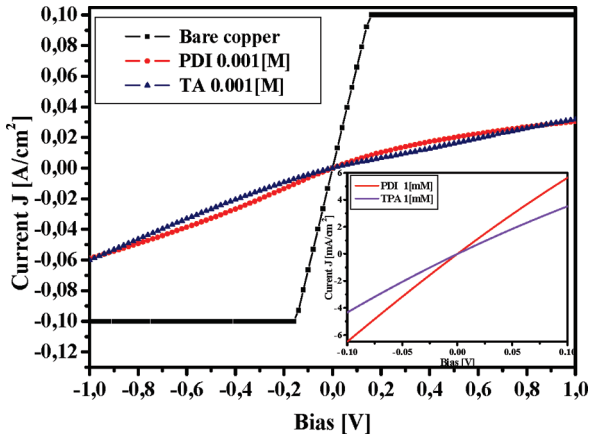

FIGURE 8. Representative current-biases, $J-V$, curves of Cu−Cu bare and molecularly modified Cu/Cu bare junctions contacted by parallel plate junction method. The data were averaged geometrically over at least 10 different samples (0.19 cm^2 area) and are presented as a single curve for each bias. The contact area of each junction was equal to the area of the Cu surface multiplied by the degree of molecular coverage. The inset depicts linear $J-V$ curves at a low bias, as expected for tunnel junctions. No hysteresis was observed during the measurements.

phenyl backbone structure and the coordination reaction between their functional groups and the Cu surface atoms. The inset of Figure 8 shows a linear behavior at the low bias range. The slightly asymmetric character of the $J-V$ curves, as can be observed from Figure 8, can be attributed mainly to the different quantity of chemical interactions between the molecular functional groups with the bottom and the top Cu electrodes.

4. SUMMARY AND CONCLUSIONS

This article describes the potential advantages of the new concept for a surface-mount placement process. The concept is based on a "bottom up" design of adhesive layer, operative in the nanometric regime through the use of self-assembled monolayers that form a protective, bridging and conductive layer between the metallic surfaces, i.e., nanopads, on one side and nanocomponents on the other side. The development of such a concept was dependent on three main factors: (i) the control of the morphology and oxidation of the bare Cu surfaces, (ii) the optimization of the self-assembled monolayer (SAM)/Cu system both in terms of the type of molecules used and in terms of the extent of coverage and protection against Cu substrate oxidation, and (iii) the creation of a stable and highly ordered SAM, binding of the SAM to a metallic overlayer and investigation of the efficiency of molecular conductivity. The first two factors were successfully covered in our previous works (8, 13, 25), and the current work focuses mainly on the third factor. The self-assembly of TPA and PDI molecules on annealed Cu surfaces were examined in detail using the information obtained from XPS, PM-IRRAS, spectroscopic ellipsometry and UHV-STM measurements. These measurements showed that the self-assembly of TPA and PDI molecules formed on top of annealed Cu creates well-ordered, high-coverage (∼90%), closely packed monolayers with a standing-up phase conformation, in which the molecules create strong coordinative reactions with the Cu substrate through one terminal functional group, with the other terminal group residing away from the substrate. The stability of both monolayers was examined at elevated temperatures (200 °C) for 1 h inside the UHV-STM system. A negligible molecular desorption during the heating modifications was observed, with more than ∼80% of the surface still covered by the SAMs in both cases. To examine the ability of these monolayers to serve as "molecular wires," i.e., the capability to provide electrical conductivity, we developed a novel fabrication parallel plate junction method to create symmetric Cu−SAM−Cu electrical junctions. This method allowed the characterization of the SAMs conductive properties in a simple and reproducible manner with a minimum of the junction defects as shorts and SAM's damage. Both SAM-modified junctions showed, as expected, almost similar current-bias characteristics, because of the similar structure and chemical interaction with the Cu substrate. These results indicated high tunneling efficiency and were in good agreement with previously reported studies of similar π-bonded molecules.

Our findings imply that the SAMs used in this study can serve as protective coatings for annealed Cu and, furthermore, as conductive molecular bridges that can potentially bind circuital pads/components in a selective manner in micro- and nanoelectronic applications.

Acknowledgment. I.P., R.T., and H.H. acknowledge the Technion's Russell Berrie Nanotechnology Institute for partial financial support. R.T. acknowledges the Israel Science Foundation (Grant 1182/09), the National Science Foundation (Award ECS-0535382) and the Marie Curie Mobility Grant from the European Union for financial support. H.H. holds the Horev Chair for Leaders in Science and Technology.

REFERENCES AND NOTES

(1) Prasad, R. *Surface Mount Technology*, 2nd ed.; Chapman & Hall: London, 1997.
(2) Tu, C.; Natishan, M. *Soldering Surf. Mount Techno.l* **2000**, *12*, 10.
(3) Wang, Y.; Olorunyomi, M.; Dahlberg, M.; Djurovic, Z.; Anderson, J.; Liu, J. *Soldering Surf. Mount Technol* **2007**, *19*, 34.
(4) Zou, L.; Dušek, M.; Wickham, M.; Hunt, C. *Soldering Surf. Mount Technol* **2003**, *15*, 35.
(5) Yang, T.; Tsai, T. *J. Intell. Manuf.* **2004**, *15*, 711.
(6) Junling, C.; Dirk, J.; Kempe, W.; Xiaoming, X. *Soldering Surf. Mount Technol* **2005**, *17*, 10.
(7) Cavallotti, P.; Zangari, G.; Sirtori, V. *J. Electron. Mater.* **1995**, *24*, 365.
(8) Platzman, I.; Saguy, C.; Brener, R.; Tannenbaum, R.; Haick, H. *Langmuir* **2010**, *26*, 191.
(9) Cano, E.; Torres, C.; Bastidas, J. *Mater. Corros.* **2001**, *52*, 667.
(10) Chawla, S.; Ricket, B.; Sankarrama, N.; Payer, J. *Corros. Sci.* **1992**, *3*, 1617.
(11) Iijima, J.; Lim, J.; Hong, S.; Suzuki, S.; Mimura, K.; Isshiki, M. *Appl. Surf. Sci.* **2006**, *253*, 2825.
(12) Suzuki, S.; Ihikawa, Y.; Isshiki, M.; Waseda, Y. *Mater. Trans. Jpn. Inst. Met.* **1997**, *38*, 1004.
(13) Platzman, I.; Brener, R.; Haick, H.; Tannenbaum, R. *J. Phys. Chem. C* **2008**, *112*, 1101.
(14) Serine, N.; Serin, T.; Karadeniz, S. *Semicond. Sci. Technol.* **2002**, *17*, 60.
(15) Chuang, C.; Aoh, J.; Din, R. *Microelectr. Reliabil.* **2006**, *46*, 449.
(16) Carel, R.; Thompson, C.; Frost, H. *Acta Mater.* **1996**, *44*, 2479.
(17) Chung, C.; Field, D.; Park, N.; Johnson, R. *Thin Solid Films* **2008**, *517*, 1977.
(18) Farkas, D.; Bringa, E.; Caro, A. *Phys. Rev. B* **2007**, *75*, 184111.

(19) Frost, H.; Thompson, C. *Curr. Opin. Solid State Mater. Sci.* **1996**, *1*, 361.
(20) Mehnert, K.; Klimanek, P. *Comput. Mater. Sci.* **1996**, *7*, 103.
(21) Miodownik, M. *Scr. Mater.* **2006**, *4*, 993.
(22) Ono, N.; Kimura, K.; Watanabe, T. *Acta Mater.* **1999**, *47*, 1007.
(23) Pranger, L.; Goldstein, A.; Tannenbaum, R. *Langmuir* **2005**, *21*, 5396.
(24) Pranger, L.; Tannenbaum, R. *J. Colloid Interface Sci.* **2005**, *292*, 71.
(25) Platzman, I.; Haick, H.; Tannenbaum, R. *Mater. Res. Soc. Symp. Proc.* **2008**, *1029*, F03.
(26) Love, J.; Estroff, L.; Kriebel, J.; Nuzzo, R.; Whitesides, G. *Chem. Rev.* **2005**, *105*, 1103.
(27) Hutt, D., C. L. *Appl. Surf. Sci.* **2005**, *252*, 400.
(28) Sinapi, F.; Lejeune, I.; Delhalle, J.; Mekhalif, Z. *Electrochim. Acta* **2007**, *52*, 5182.
(29) Jennings, G.; Munro, J.; Yong, T.-H.; Laibinis, P. *Langmuir* **1998**, *14*, 6130.
(30) Salomon, A.; Cahen, D.; Lindsay, S. M.; Tomfohr, J.; Engelkes, V. B.; Frisbie, C. D. *Adv. Mater.* **2003**, *15*, 1881.
(31) Haick, H.; Ambrico, M.; Ligonzo, T.; Tung, R. T.; Cahen, D. *J. Am. Chem. Soc.* **2006**, *128*, 6854.
(32) James, D.; Tour, J. *Chem. Mater.* **2004**, *16*, 4423.
(33) Yamane, H.; Yabuuchi, Y.; Fukagawa, H.; Kera, S.; Okudaira, K.; Ueno, N. *J. Appl. Phys.* **2006**, *99*, 093705/1.
(34) Nijhuis, C.; Reus, W.; Whitesides, G. *J. Am. Chem. Soc.* **2009**, *191*, 17814.
(35) Haick, H.; Cahen, D. *Acc. Chem. Res.* **2007**, *41*, 359.
(36) Haick, H.; Cahen, D. *Prog. Surf. Sci.* **2008**, *83*, 217.
(37) Holloway, K.; Fryer, P.; Cabral, C.; Harper, J.; Bailey, P.; Kelleher, K. *J. Appl. Phys.* **1992**, *71*, 5433.
(38) Ou, K.; Wu, W.; Chou, C.; Chiou, S.; Wu, C. *J. Vac. Sci. Technol., B* **2002**, *20*, 2154.
(39) Golden, W.; Saperstain, D. *J. Electron. Spectrosc.* **1983**, *30*, 43.
(40) Palik, E. E. *Handbook of Optical Constants of Solids*; Academic Press: New York, 1985.
(41) Yoshitoki, I.; Noriyasu, N.; Kenzo, H. *Surf. Interface Anal.* **1996**, *24*, 93.
(42) Shirley, D. *Phys. Rev. B.* **1972**, *5*, 4709.
(43) Dulot, F.; Eugène, J.; Kierren, B.; D., M. *Appl. Surf. Sci.* **2000**, *162–163*, 86.
(44) Moulder, J.; Stickle, W.; Sobol, P.; Bomben, K. *Handbook of X-ray Photoelectron Spectroscopy*; Perkin-Elmer Corp.: Eden Prairie, MN, 1992.
(45) Briggs, D.; Seah, M. *Practical Surface Analysis- Auger and X-ray Photoelectron Spectroscopy*, 2nd ed.; Wiley Interscience: Chichester, U.K., 1990.
(46) Cañas-Ventura, M.; Klappenberger, F.; Clair, S.; Pons, S.; Kern, K.; H., B. *J. Chem. Phys.* **2006**, *125*, 184710.
(47) Deng, X.; Verdaguer, A.; Herranz, T.; Weis, C.; Bluhm, H.; Salmeron, M. *Langmuir* **2008**, *24*, 9474.
(48) McCafferty, E.; Wightman, J. *Surf. Interface Anal.* **1998**, *26*, 549.
(49) Dubot, P.; Jouset, D.; Pinet, V.; Pellerin, F.; Langeron, J. *Surf. Interface Anal.* **1988**, *12*, 99.
(50) Yamamoto, Y. *Coord. Chem. Rev.* **1980**, *32*, 193.
(51) Han, H.; Han, S.; Joo, S.; Kim, K. *Langmuir* **1999**, *15*, 6868.
(52) Varsanyi, G. *Assignments for Vibrational Spectra of Seven Hundred Benzene Derivatives*; Wiley: New York, 1974.
(53) Tour, J.; Jones, L.; Pearson, D.; Lambda, J.; Burgin, T.; Whitesides, G.; Allara, D.; Parikh, A.; Atre, S. *J. Am. Chem. Soc.* **1995**, *117*, 9529.
(54) Kim, H.; Lee, S.; Kim, N.; Yoon, J.; Park, H.; Kim, K. *Langmuir* **2003**, *19*, 6701.
(55) Sexton, B.; Avery, N. *Surf. Sci.* **1983**, *129*, 21.
(56) Ellison, M.; Hamers, R. *J. Phys. Chem. B* **1999**, *103*, 6243.
(57) Lin, S.; McCarley, R. *Langmuir* **1999**, *15*, 151.
(58) Tao, Y.; Lee, M.; Chang, S. *J. Am. Chem. Soc.* **2003**, *115*, 9547.
(59) Henderson, J.; Feng, S.; Bein, T.; Kubiak, C. *Langmuir* **2000**, *16*, 6183.
(60) Swanson, S.; McClain, R.; Lovejoy, K.; Alamdari, N.; Hamilton, J.; Scott, J. *Langmuir* **2005**, *21*, 5034.
(61) de Boer, B.; Frank, M. M.; Chabal, Y. J.; Jiang, W.; Garfunkel, E.; Bao, Z. *Langmuir* **2004**, *20*, 1539.
(62) Haick, H.; Ghabboun, J.; Cahen, D. *Appl. Phys. Lett.* **2005**, *86*, 042113/1.
(63) Haynie, B. C.; Walker, A. V.; Tighe, T. B.; Allara, D. L.; Winograd, N. *Appl. Surf. Sci.* **2003**, *203–04*, 433.
(64) Lu, P.; Walker, A. *Langmuir* **2007**, *23*, 12577.
(65) Haick, H.; Ghabboun, J.; Niitsoo, O.; Cohen, H.; Cahen, D.; Vilan, A.; Hwang, J.; Wan, A.; Amy, F.; Kahn, A. *J. Phys. Chem. B* **2005**, *109*, 9622.
(66) Jung, D. R.; Czanderna, A. W.; Herdt, G. C. *J. Vac. Sci. Technol. A* **1996**, *14*, 1779.
(67) Ohgi, T.; Sheng, H.-Y.; Dong, Z.-C.; Nejoh, H. *Surf. Sci.* **1999**, *422*, 277.
(68) Haick, H.; Ambrico, M.; Ghabboun, J.; Ligonzo, T.; Cahen, D. *Phys. Chem. Chem. Phys.* **2004**, *6*, 4538.
(69) Haick, H.; Niitsoo, O.; Ghabboun, J.; Cahen, D. *J. Phys. Chem. C* **2007**, *111*, 2318.
(70) Oskam, G.; Long, J.; Natarajan, A.; Searson, P. *J. Phys. D* **1998**, *31*, 1927.
(71) Schneeweiss, M.; Kolb, D. *Phys. Status Solidi. (a)* **1999**, *173*, 51.
(72) Sondag-Huethorst, J.; Fokkink, L. *Langmuir* **1995**, *11*, 4823.
(73) Hagenström, H.; Schneeweiss, M.; Kolb, D. *Electrochim. Acta* **1999**, *45*, 1141.
(74) Baunach, T.; Kolb, D. *Anal. Bioanal. Chem.* **2002**, *373*, 743.
(75) Cavalleri, O.; Gilbert, S.; Kern, K. *Surf. Sci.* **1997**, *377–79*, 931.
(76) Esplandiu, M.; Hagenstrom, H. *Solid State Ionics* **2002**, *150*, 39.
(77) Loo, Y. L.; Lang, D. V.; Rogers, J. A.; Hsu, J. W. P. *Nano Lett.* **2003**, *3*, 913.
(78) Loo, Y.-L.; Willett, R. L.; Baldwin, K. W.; Rogers, J. A. *J. Am. Chem. Soc.* **2002**, *124*, 7654.
(79) Hsu, J. W. P. *Mater. Today* **2005**, *8*, 42.
(80) Guerin, D.; Merckling, C.; Lenfant, S.; Wallart, X.; Pleutin, S.; Vuillaume, D. *J. Phys. Chem. C.* **2007**, *111*, 7947.

AM100427A